ACOUSTIC EMISSION ANALYSIS FOR THE DETECTION OF APPROPRIATE CUTTING OPERATIONS IN HONING PROCESSES

Irene Buj-Corral[1,*] Jesús Andrés Álvarez-Flórez[2], and Alejandro Domínguez-Fernández[1]

[1] Department of Mechanical Engineering, Universitat Politècnica de Catalunya, Av. Diagonal, 647, 08028 Barcelona, Spain

[2]Heat Engines Department, Universitat Politècnica de Catalunya, Av. Diagonal, 647, 08028 Barcelona, Spain

*Corresponding author. Tel. +34934054016. Fax. +34934016693.

E-mail address: irene.buj@upc.edu (I. Buj)

Abstract

In the present paper, acoustic emission was studied in honing experiments obtained with different abrasive densities, 15, 30, 45 and 60. In addition, 2D and 3D roughness, material removal rate and tool wear were determined. In order to treat the sound signal emitted during the machining process, two methods of analysis were compared: Fast Fourier Transform (FFT) and Hilbert Huang Transform (HHT). When density 15 is used, the number of cutting grains is insufficient to provide correct cutting, while clogging appears with densities 45 and 60. The results were confirmed by means of treatment of the sound signal. In addition, a new parameter S was defined as the relationship between energy in low and high frequencies contained within the emitted sound. The selected density of 30 corresponds to S values between 0.1 and 1. Correct cutting operations in honing processes are dependent on the density of the abrasive employed. The density value to be used can be selected by means of measurement and analysis of acoustic emissions during the honing operation. Thus, honing processes can be monitored without needing to stop the process.

Keywords: honing; acoustic emission; roughness; material removal rate; Hilbert Huang transform; Fourier transform

1 Introduction

As a general trend, machine tool users choose CBN (cubic boron nitride) tools for machining hard materials like the hardened steel used in molds. Although they are quite expensive, they allow high material removal rate with low wear [1]. This is also the case for abrasive tools. In grinding processes, if grit volume or density is reduced , weaker structures are obtained for grinding wheels [2]. Grit concentration is related to the number of active surfaces that will enhance material removal rate. In addition, higher concentrations are associated with lower chip thicknesses and lower roughness [3]. As for honing processes, in industry, the selection of grain

size depends mainly on the type of process to be used: rough, semi-finish or finish honing. After selecting the grain size, the abrasive density is also defined. Once the honing stone has been selected, several tests are performed in which pressure, linear speed and tangential speed are varied, in order to obtain the appropriate roughness, material removal rate and tool wear [4]. If the selected density is too low, tools will suffer premature wear and will show low productivity, regardless of the cutting conditions employed. Since CBN abrasives are expensive, high densities are usually preferred in order to increase productivity, in the same way as for grinding. However, an excessively high density will not allow proper material cutting, because of clogging of the honing tool.

The shape of acoustic waves produced in abrasive machining processes depends largely on whether the cutting tool is cutting properly or not. In the past, several authors have used acoustic emission for determining tool failure in different machining processes [5], [6], including grinding [7]. In abrasive processes such as grinding, wavelet packet transform of acoustic emission has been used for detecting grinding burn [8]. Acoustic emission also allowed measuring the wheel-workpiece contact length in grinding operations [9]. The amplitude of the sound signal is known to vary with different cutting conditions in the grinding processes [10]. As for the honing processes, few papers are known. For example, Schmitt et al. measured acoustic emissions on different surfaces although they did not find significant differences among the signals measured [11]. Kanthababu et al. monitored acoustic emission for rough, semi-finish and plateau honing for fresh and worn out tools. They found that the dominant frequency of the signal is sensitive to the cutting conditions [12]

The acoustic signal is usually analysed in the frequency domain, by means of Fast Fourier Transform (FFT), and also in the time-frequency domain (TFS) [13]. Other time-frequency (TF) methods are available for analysing the acoustic signal, such as Hilbert Huang Transform (HHT) and wavelet transform. Hilbert Huang Transform (HHT) decomposes nonstationary signals obtained from nonlinear systems in individual oscillatory modes [14]. It allows analysing nonlinear and nonstationary signals. In the wavelet transform, a family of translates

and dilates of one basic primitive mother wavelet is used [15]. As a result of the computational processes, it is possible to obtain the spectrogram (TF plane), the scalogram (TS plane), and the smoothed Wigner-Ville distribution [16]. Nevertheless, wavelet is not appropriate for nonlinear signals. It is usually employed for linear but nonstationary signals.

Several time-frequency (TF) methods have been used in the past for analysing nonstationary or stationary signals with high nondeterministic components, such as those obtained in this work. The time-frequency-scale (TFS) transform concept has been used, for example, for monitoring the milling process and detecting surface irregularities [17]. Wavelet transform allowed finding material damage in civil infrastructures [18,19] or in wind blades [20], as well as detecting low speed bearing failure [21]. Hilbert-Huang Transform (HHT) has also been used for determining the mechanical properties of refractory materials [22]. As for machining processes, HHT has been applied to detect tool breakage [23,24] and chatter [25,26]. However, most papers address milling processes. Regarding abrasive processes, HHT was applied to detect the burn feature in grinding operations [27]. In contrast, few papers are known about the application of HHT to honing.

In the present paper, semi-finish honing tests were performed at different abrasive densities. In order to detect correct cutting, 2D roughness, material removal rate and tool wear were used in the first analysis. A more refined analysis involved determining 3D roughness and surface topographies. Once the most appropriate density had been selected, the acoustic emission of the honing process was analysed by means of two methods, Fast Fourier Transform (FFT) and Hilbert Huang Transform (HHT). A new parameter S was defined, which allows the proper abrasive cutting operation to be determined. It will provide a quick way of determining whether the abrasive is cutting properly or not, without needing to analyse the surface finish of the workpiece nor the final state of the abrasive. This monitoring of the honing process will lead to a reduction in the number of tests and abrasive stones that are required in previous honing tests.

2 Materials and methods

2.1 Honing experiments

The honing machine used was an experimental equipment composed by an oscillating table, with acceleration up to 4.9 m/s^2, on which a honing stead provided with three tool supports is placed (Figure 1). The table moves thanks to a linear motor.

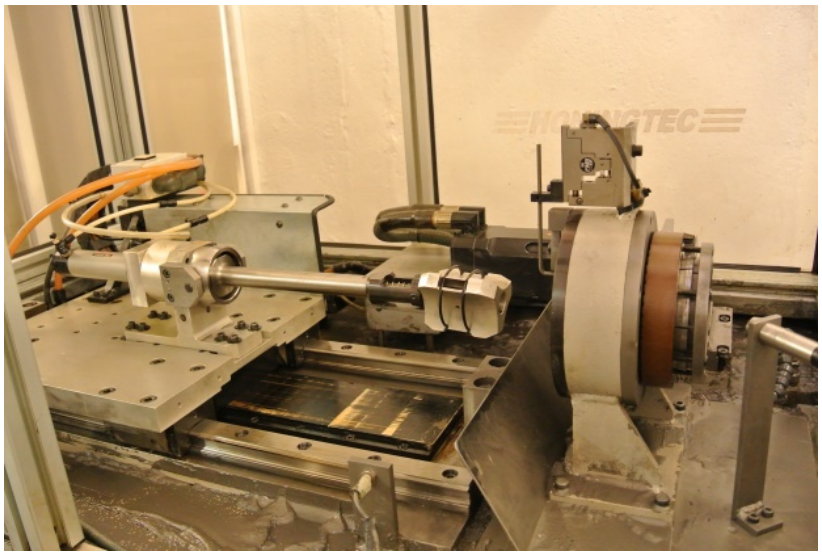

Figure 1. Honing machine

The rotation movement is applied to the cylinders, by means of a rotary motor and a belt transmission (Figure 2).

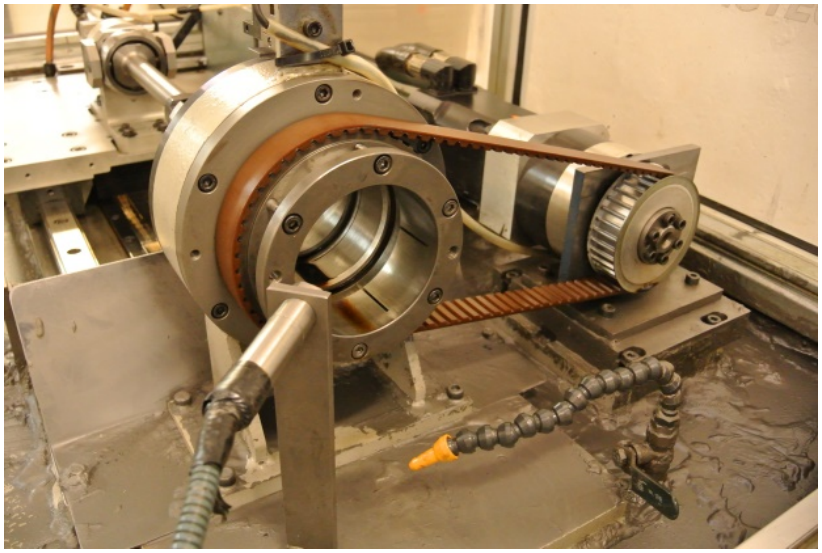

Figure 2. Motor and transmission for workpiece rotation

Pressure of the honing stones against workpiece wall is provided by a pneumatic cylinder, provided with a pressure sensor, an electrovalve that controls pneumatic pressure.

Steel St-52 cylinders of internal diameter 80 mm and length 100 mm were used in the honing tests. The honing machine used was a prototype in which the workpiece rotates, providing tangential speed, and the honing head has a linear reciprocating movement, leading to linear speed. Oil was used as cutting fluid. CBN stones with metal bond were employed. Abrasive stone dimensions are 20 mm x 3 mm x 3 mm.

Experimental tests performed are listed in Table 1. Grain size GS, tangential speed VT, linear speed VL and pressure against the workpiece wall PR were fixed, while censity of abrasive DE was varied. Two replicates were performed of each experiment.

Table 1 Experiments performed

Experiment	GS (FEPA[28])	DE (ISO6104 [29])	PR ($N \cdot cm^{-2}$)	VT ($m \cdot min^{-1}$)	VL ($m \cdot min^{-1}$)
700-15	64	15	700	40	30
700-30	64	30	700	40	30
700-45	64	45	700	40	30
700-60	64	60	700	40	30

Experiments were named using the pressure value followed by the density value. For example, 700-15 stands for an experiment with pressure 700 N/cm^2 and density of abrasive 15 according to the Federation of European Producers of Abrasives (FEPA) nomenclature.

2.2 Roughness, material removal rate and tool wear measurement

Average roughness Ra, areal average roughness Sa, areal average distance between the highest peak and lowest valley in a sampling length St, areal skewness Ssk, areal kurtosis Sku and surface topographies were obtained with a Taylor Hobson Talysurf Series 2 roughness meter. Material removal rate was determined by means of the weight of the workpiece before and after the honing operation. Tool wear was calculated by the weight of the honing stones before and

after each honing test. Pictures of the honing stones were obtained with a Leica S8AP0 magnifier, with x80 magnification.

2.3- Sound signal analysis

Acoustic emission was recorded during the machining process by means of a piezoelectric microphone Senheiser MM30G for audio applications with frequency range 40 Hz – 20 KHz. The microphone was positioned in the machine wall near the cutting area but protected from cutting oil. Afterwards, the obtained signals were analysed by means of two different methods: FFT and TFS plus HHT. Evaluation software was Matlab 2013a.

The first method for analysing the sound signals $x(t)$ was with Fourier coefficients C_k (Eq. 1), obtained by means of Fast Fourier transform (FFT).

$$C_k = \frac{1}{T_p}\int_0^{T_p} x(t)e^{-j2\pi kF_0 t}\,dt \quad \text{(Eq. 1)}$$

$$k = 0, \pm 1, \pm 2, \ldots$$

Where T_p is the period of signal and F_0 is its fundamental frequency.

With these coefficients the re-synthesis to the original signal is possible, using Eq. 2.

$$x(t) = \sum_{k=-\infty}^{\infty} C_k e^{j2\pi kF_0 t} \quad \text{(Eq. 2)}$$

$$k = 0, \pm 1, \pm 2, \ldots$$

The second method needed, for finer sound signal analysis, was the use of time-frequency-scale transform (TFS) and Hilbert Huang Transform (HHT).

In order to simultaneously solve the uncertain visualization of events occurring over time and their frequencies, the time-frequency-scale (TFS) transform concept was needed. The short-term Fourier transform (STFT) was computed, by gradually varying the window size used each time. Spectrograms were obtained with 128 samples as window value, 64 samples as overlap value, and 512 as the number of sampling points needed to calculate the discrete Fourier transform.

The Hilbert-Huang method was structured in two steps. The first corresponds to Empirical Mode Decomposition (EMD). Afterwards, Hilbert analysis is used as a second step. EMD provides a family of signals organised into different frequency ranges, known as Intrinsic Mode Functions (IMF), to which the Hilbert transform is applied in order to show the instantaneous frequency over time.

IMFs need to comply with certain rules, such as having the same number of zero-crossing and extrema and symmetric envelopes in the local maxima and minima. They are obtained with a numerical recursive algorithm applied to the original signal *x(t)* (Eq. 3).

$$x(t) = \sum_{i=1}^{n} IMF_i(t) + R_n(t) \qquad \text{(Eq. 3)}$$

Where IMF_i(t) are n decomposition new functions,

and *Rn* is a final residue, characterized by a constant, a monotonic function or a function with only one maximum and minimum.

In this case study, 15 IMF's were obtained by the EMD method. The first IMF contains the highest frequency component, and the last IMF contains the lowest one. This decomposition of the original signal allows for more refined analyses, in every frequency band, than FFT, Wavelets or Hilbert Transform.

So, for every IMF considered as a new temporary signal, the Hilbert transform is applied in order to visualize the instantaneous frequency over time. The analytical signal $s_i(t)$ is obtained with Equation 4, where $S_i(t)$ is the Hilbert transform of $IMF_i(t)$ as a convolution with $h = 1/\pi t$ (Eq. 5).

$$s_i(t) = IMF_i(t) + jS_i(t) \qquad \text{(Eq. 4)}$$

$$S_i(t) = (h * IMF)(t) = \frac{1}{\pi}\int_{-\infty}^{\infty} \frac{IMF(\tau)}{t-\tau} d\tau \qquad \text{(Eq. 5)}$$

3 Results

3.1 2D surface roughness, material removal rate and tool wear.

Average Roughness (Ra), Material Removal Rate (MRR) and Tool Wear are presented in Figure 3 as a function of the abrasive density.

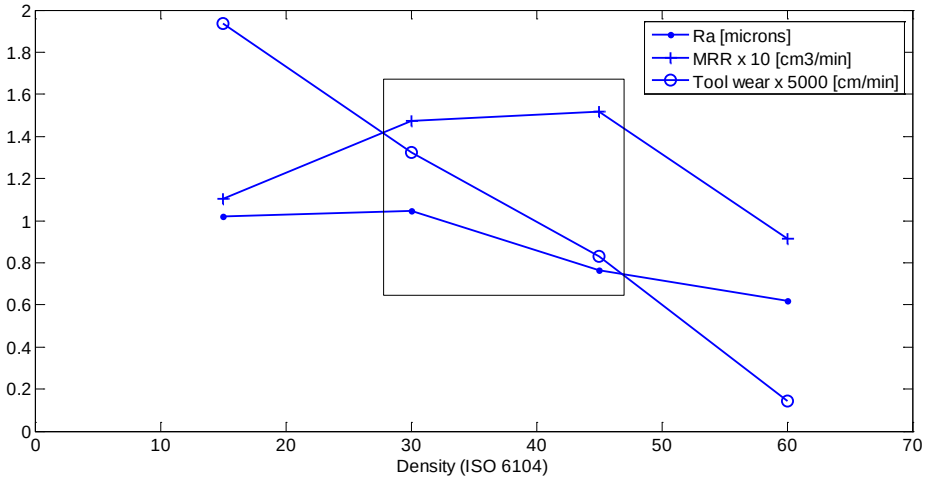

Figure 3. Average roughness Ra, Material Removal Rate MRR and tool wear vs. Abrasive density

From density 30 onward, the higher the density, the lower the roughness. Since the same grain size of abrasive was used in all cases, this suggests saturation or clogging of abrasive stones because of a lack of space for the removed chips. Material removal rate, MRR, increases with density of up to 45, which shows relatively low roughness and tool wear. For density 60, clogging is so significant that the honing stone loses its ability to remove material, with the lowest MRR value. As expected, tool wear is inversely proportional to abrasive density. For a high density value of 60, tool wear is negligible. Since clogging occurs, the abrasive grains do not work properly and, for this reason, the abrasive does not wear significantly.

In Figure 4 the abrasive surface is depicted after different honing tests, with magnification x80.

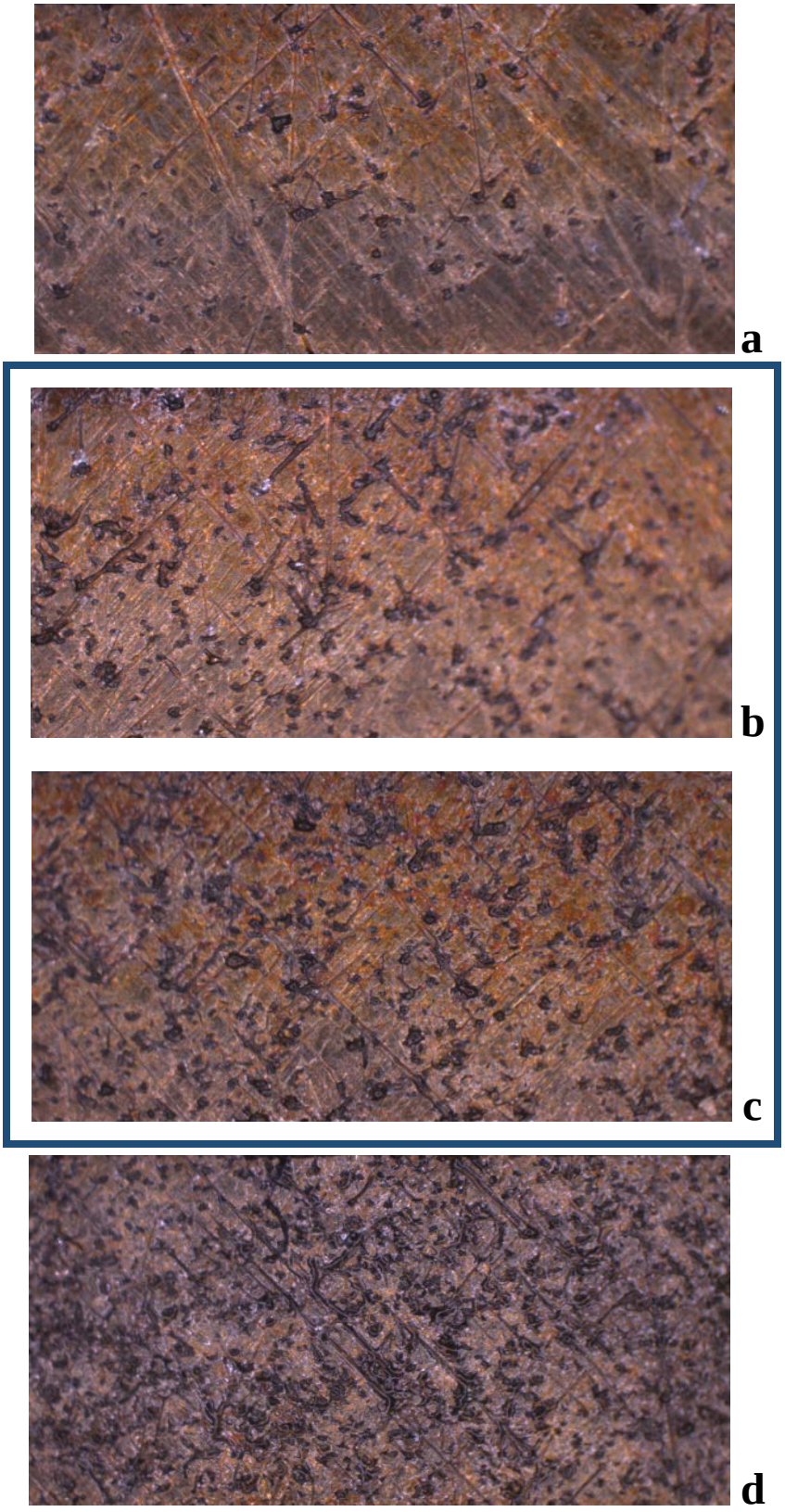

Figure 4. Pictures of abrasive surface after honing tests: a) 700-15, b) 700-30, c) 700-45, d) 700-60

Figure 2a corresponds to density 15. Some marks are observed on the stone's surface in a different direction to that of the honing. This may be due to the fact that abrasive particles are removed easily from the stone surface and remain between the stone and the workpiece's surface, producing long marks. In Figure 2b, obtained with density 30, some short marks are observed in a different direction to that of the honing, with a proper cutting operation. In Figure 3c, with density 45, some short marks are also present, suggesting the correct behaviour of the honing stone. In Figure 2d, with density 60, some long marks are observed in a different direction to that of the honing, which may be attributed to loose chips that remain out of the stone surface because of clogging.

According to Figures 1 and 2, densities 30 and 45 would correspond to proper cutting operation. However, a more detailed analysis is presented in section 3.2, taking 3D roughness into account.

3.2 3D surface roughness.

In order to investigate whether the surface topographies obtained with different densities of abrasive are homogeneous, a 3D roughness measurement was performed.

Figure 5 shows the resulting images of the 3D roughness measurement. Surface topographies correspond to an area of 1 x 1 mm.

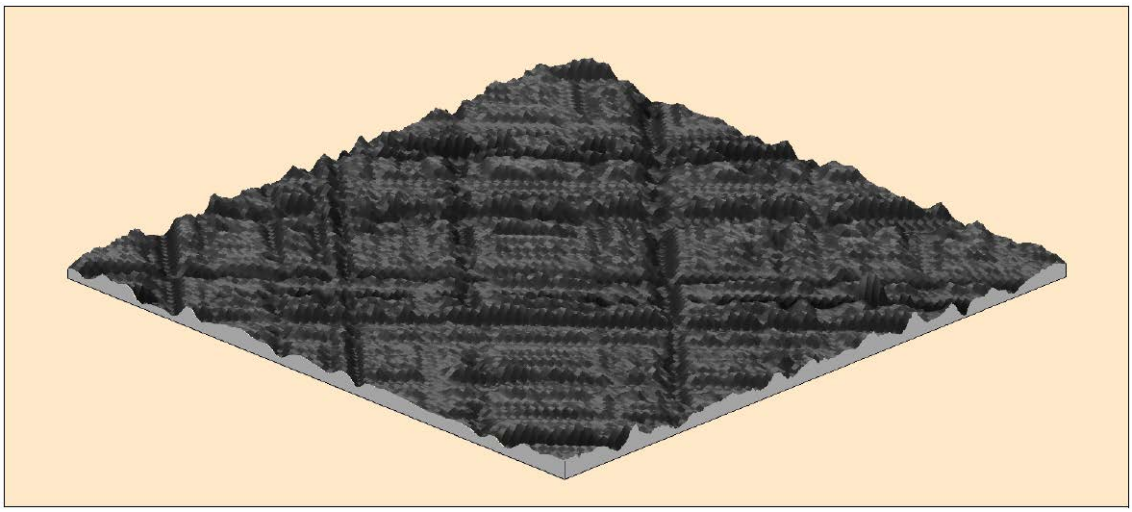

a

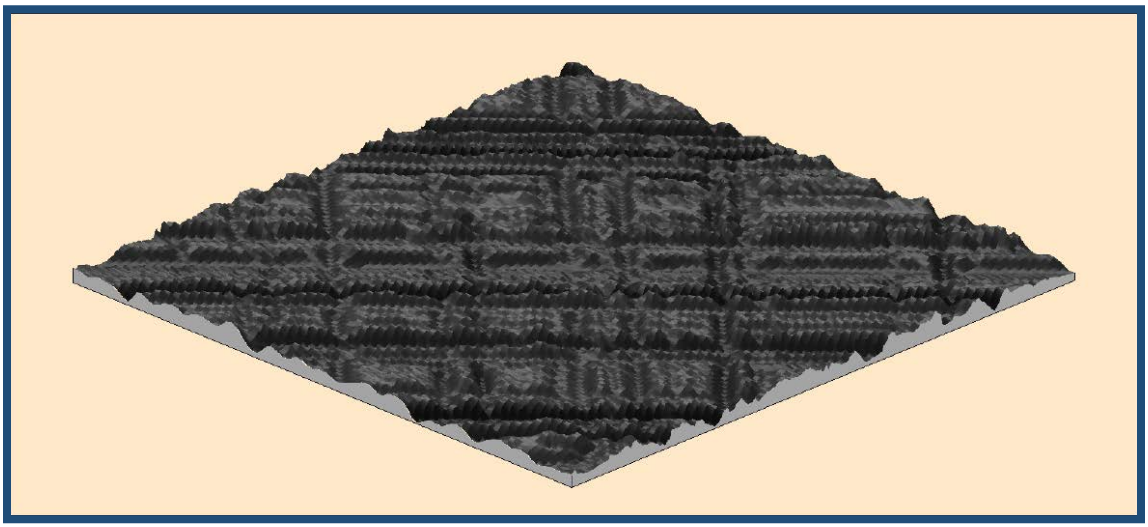

b

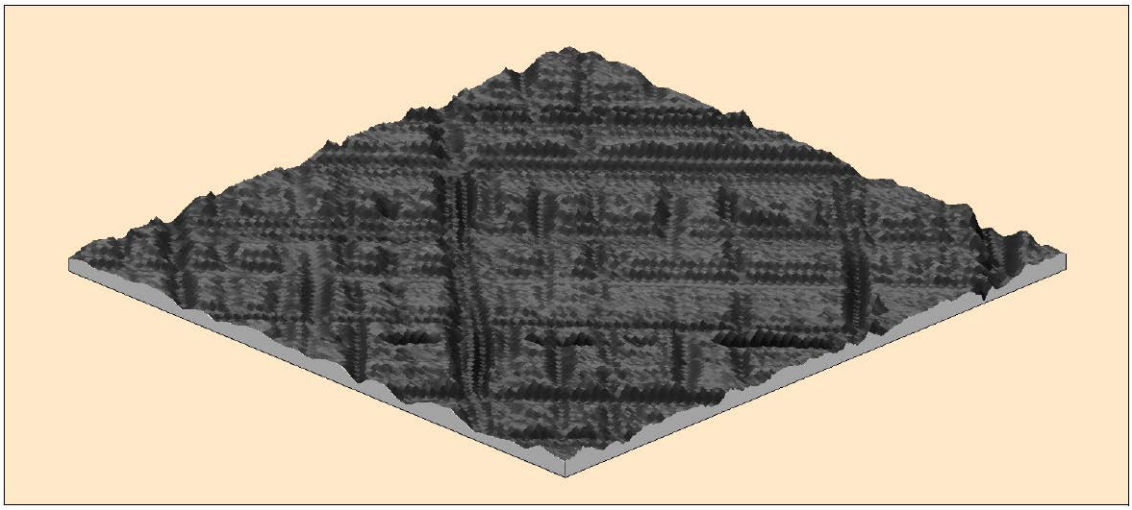

c

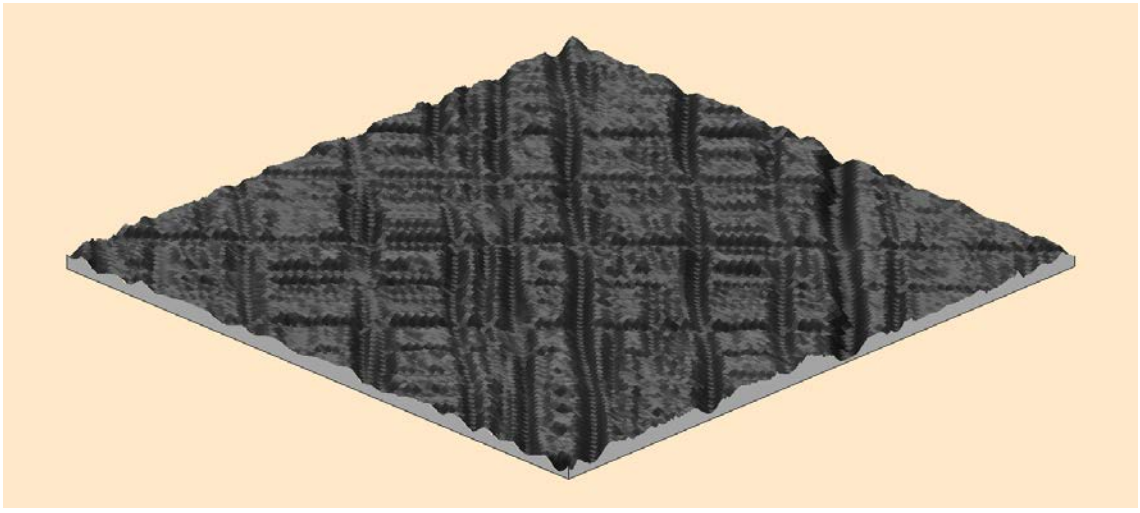

d

Figure 5. Resulting images of the 3D roughness measurement: a) 700-15, b) 700-30, c) 700-45, d) 700-60.

In Figure 5a, obtained with density 15, few cutting marks are observed within the studied area, although they are continuous and straight. Figure 5b, obtained with density 30, shows a higher number of marks, with a more homogeneous surface, still with straight cutting marks. In Figure 5c, obtained with a higher abrasive density of 45, discontinuous marks are observed, with a little curvature, suggesting some saturation of the abrasive stone. When density 60 was used (Figure 5d), many non-straight marks are observed in one direction of the cross-hatch pattern, with shallower discontinuous marks in a perpendicular direction. In addition, flatter peaks are observed, the results of an important clogging process in which the abrasive stone cuts the material with more difficulty.

Table 2 contains the areal roughness parameter values for the different experiments performed.

Table 2 Areal roughness parameters for the different experiments performed

Experiment	Sa (μm)	Sz (μm)	Ssk	Sku
700-15	1.04	9.68	0.21	3.62
700-30	1.02	8.86	0.01	3.26
700-45	0.79	9.87	-0.21	4.19
700-60	0.70	7.36	-0.36	3.80

The areal average roughness parameter Sa decreased significantly with abrasive density of 30 onward, as was previously observed for 2D parameter Ra in Figure 3. The Sz parameter is higher than 8.8 for densities 15, 30 and 45, while it decreases to 7.36 for density 60, suggesting

that clogging of the honing stone flattens the ridges of the surface topography. Parameter Ssk, which is related to the symmetry of the surface topography, is higher than 0 for density 15, has a value close to zero for density 30 and is negative for densities 45 and 60. Thus, when abrasive density is too low, peaks are more important than valleys; when density is too high and clogging is observed, valleys are more important than peaks. Finally, a symmetric topography is obtained when the honing operation is correct. In addition, the value of Sku or kurtosis for density 30 is close to 3, corresponding to a normal distribution of roughness heights. In short, 3D roughness measurements indicate that 30 is the best abrasive density, taking into account the homogenous surface and a higher number of marks in comparison with density 45, as well as the areal roughness parameters.

Surface finish, material removal rate and tool wear all need to be determined after the honing process is performed. Section 3.3 presents the analysis of acoustic emission, which allows the honing process to be monitored while it is being executed.

3.3 Time and frequency domain signals

Figure 6 shows the acoustic signal of honing experiments over time for different operations. By visualizing the signals it is possible to establish a first preliminary correlation between abrasive density and emitted sound, since higher density corresponds to greater sound level variation in the time domain.

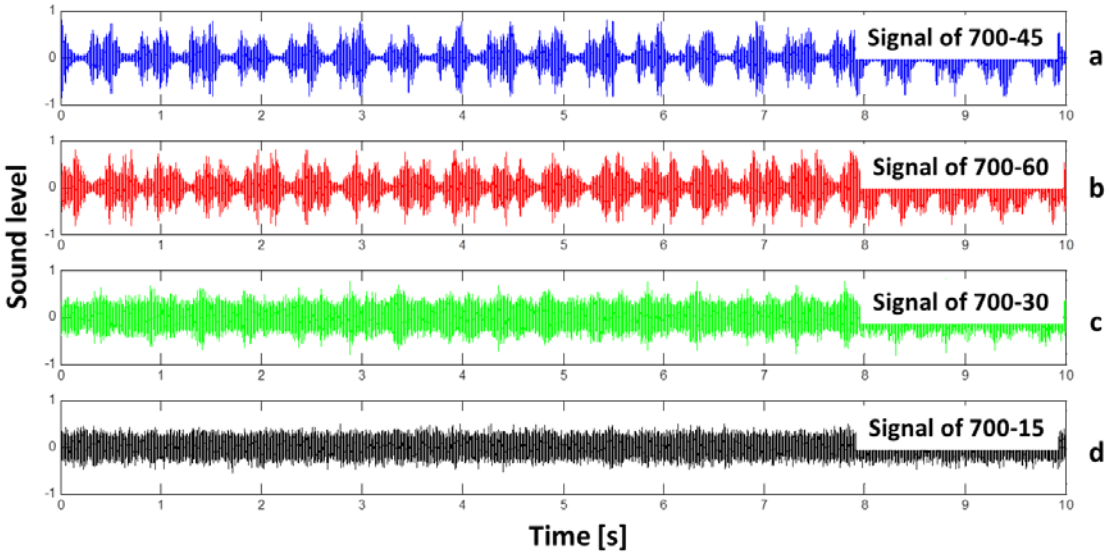

Figure 6. Sound signals in time domain obtained during machining process: a) 700-45, b) 700-60, c) 700-30 and d) 700-15

For low density values of 700-15 and 700-30, Figures 6d and 6c respectively, apparent periodic signals are not observed and only some apparent noise can be detected. For high density values of 700-45 and 700-60, Figures 6a and 6b respectively, a significant variation of sound level is present, which is maintained over time.

Analysis of the signals in the frequency domain by FFT is shown in Figure 5, with no significant peaks and level at frequencies higher than 2500 Hz. Two frequency bands, depending on energy distribution, can be established: from 0 to 1000 Hz and from 1000 to 2500 Hz. Looking at the two different frequency bands, significant differences can be observed in the four experiments studied.

Acoustic energy is concentrated in the 1000 to 2500 Hz band for high abrasive density (Figures 7a and 7b). In contrast, when low density abrasives are machined (Figures 7c and 7d), acoustic energy is mostly present in the 0 to 1000 Hz band, with peaks of lesser amplitude between 1000 and 2500 Hz.

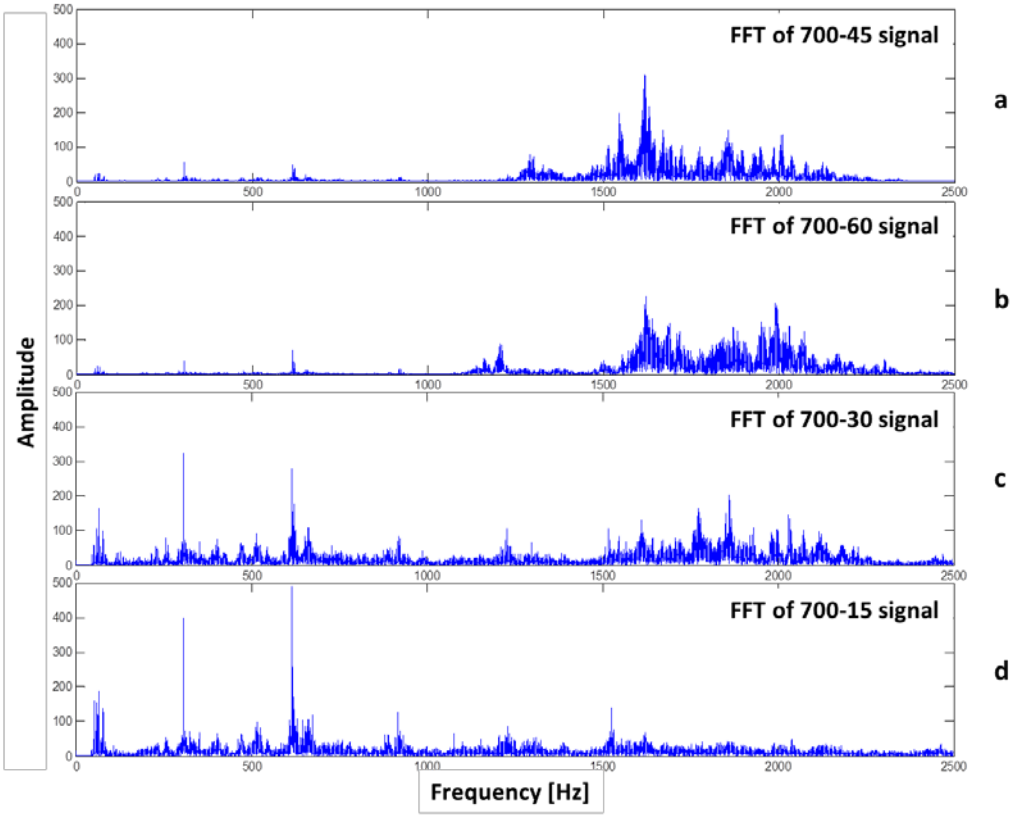

Figure 7. Sound signals in frequency domain 0-2500 Hz:

a) 700-45, b) 700-60, c) 700-30 and d) 700-15

The presence of two different groups of peaks suggests that the relationship between the energy of a low frequency signal, below 1000 Hz, and that of a high frequency signal, above 1000 Hz, is important. Thus, a new parameter, $S_{F,}$ was defined for analyzing the signal (Equation 6).

$$S_F = \frac{Lf}{Hf} \qquad \text{(Eq. 6)}$$

Where *Lf* is the energy of the FFT signal at low frequency bands (0-1000 Hz), and *Hf* is the energy of the FFT signal at high frequency bands (1000-2500 Hz).

Assuming that almost all the signal's energy is contained between 0 to 2500 Hz, by applying Parseval's theorem it is possible to calculate, the two mentioned frequency bands, using Equation 7.

$$P_x = \frac{1}{T_p}\int_0^{T_p}|x(t)|^2 dt = \frac{1}{N_{-\infty}^{-1}}\sum_{k=-\infty}^{-1}|C_k|^2 + \frac{1}{N_0^{1000}}\sum_{k=0}^{1000}|C_k|^2 + \frac{1}{N_{1001}^{2500}}\sum_{k=1001}^{2500}|C_k|^2 + \frac{1}{N_{2501}^{\infty}}\sum_{k=2501}^{\infty}|C_k|^2 \quad \text{(Eq. 7)}$$

$$k = 0, \pm 1, \pm 2, \ldots$$

Where P_x corresponds to the energy of the sound signal $x(t)$ in the analysis interval (5 seconds), C_k corresponds to the Fourier coefficients, and

T_p is the period of signal obtained from fundamental frequencyF_0.

Lf and Hf values can be calculated according to Equation 8 and Equation 9 respectively.

$$Lf = \frac{1}{1000}\sum_{k=0}^{1000}|C_k|^2 \qquad \text{(Eq. 8)}$$

$$Hf = \frac{1}{1500}\sum_{k=1001}^{2500}|C_k|^2 \qquad \text{(Eq. 9)}$$

Table 3 shows Lf, Hf , S_F and the total energy for the different experiments.

Table 3. Lf, Hf, S_F and energy for the different experiments performed

Experiment	Lf	Hf	S_F	Total Energy
700-45	$2.06e^{-4}$	0.0224	0.0092	0.0226
700-60	$1.44e^{-4}$	0.0267	0.0037	0.0268
700-30	0.0065	0.0168	0.39	0.0234
700-15	0.0088	0.0052	1.69	0.0140

High S_F value, for example 1.69 obtained for experiment 700-15, implies that the energy signal is balanced in the low frequency domain, suggesting that abrasive density is too low and the stones are not able to cut enough material. This corresponds to low MRR and high Ra, according to Figure 1. Total energy value is low. On the contrary, low S_F values of 0.037 and

0.0092 were reported for experiments 700-60 and 700-45 respectively, with high abrasive density. In this case, the energy signal is concentrated mainly in the high frequency domain, with a higher total energy value. Best results were found for the medium S_F value of 0.39 (experiment 700-30), where there are peaks at both high and low frequencies, because there are enough abrasive grains to cut but clogging has not yet appeared.

As a preliminary conclusion, of the four experiments the best one has S_F values between 0.1 and 1.

3.4 Time-frequency analysis by Hilbert Huang transform

A finer analysis of the information included in the acoustic signal emitted during the honing process is possible by means of the determination of the patterns contained in the time-frequency representation of the signal.

In Figure 8, the time-frequency representation obtained from the first IMF for all experiments is represented by a thin blue line, over 5 seconds of time. Since the IMF frequency presents a high variation, a smoothing treatment is needed. Thus, the mean from shifting τ samples windowed, like a moving average filter (according to Equation 10) is shown by a thick red line. It allows the time-frequency trend of the signal to be obtained.

$$y_i(n) = \frac{1}{w}\sum_{\tau=n}^{n+w} IMF_i(\tau) \qquad \text{(Eq. 10)}$$

$$1 < n < (n-\tau)$$

Where $y_1(n)$ is the function for the mean from shifting windowed samples for every experiment, in which the window used, w, had 100 samples.

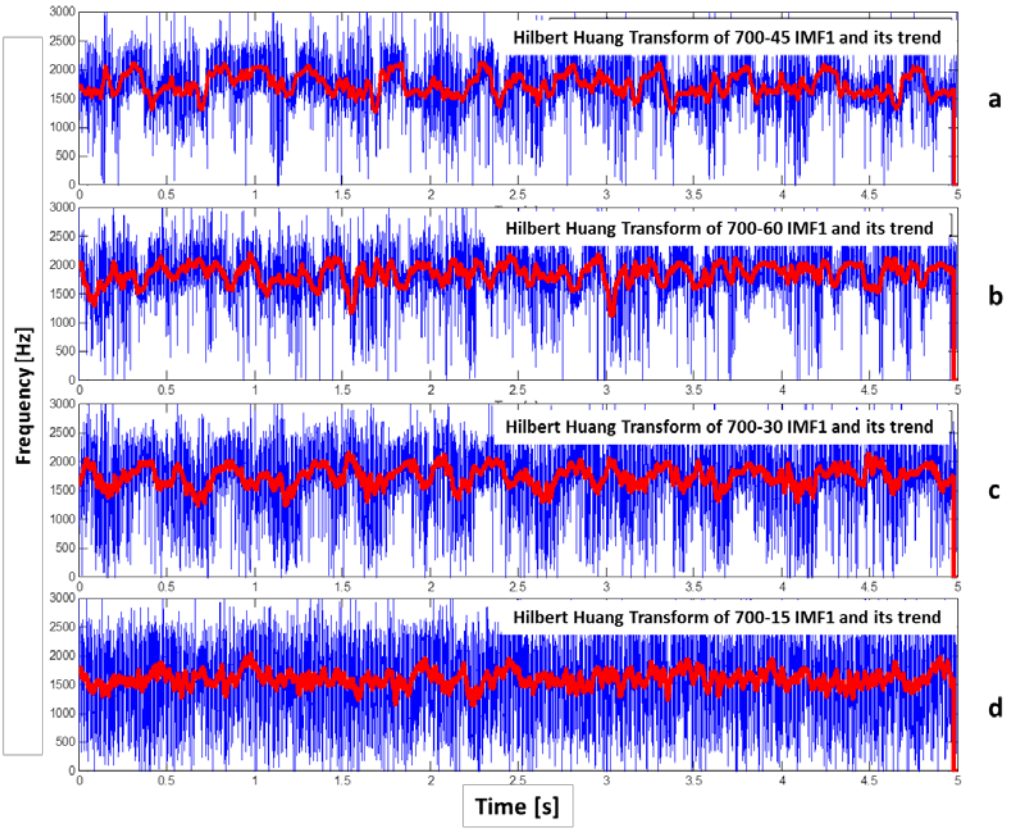

Figure 8. Time-frequency representation over a period of 5 s, corresponding to 1rst IMF component from EMD treatment: a) 700-45, b) 700-60, c) 700-30 and d) 700-15

As the abrasive density decreases, the acoustic effect of the cutting process is substituted by the acoustic effect of friction of abrasives with the material. At density 15 (Figure 8d), time-frequency representation shows wider amplitudes at all times, with a narrower range for the red line than for density 30 (Figure 8c). As density increases, narrow and wide amplitudes coexist, suggesting clogging (Figures 8a and 8b), with a wider range for the red line.

From the red line pattern obtained, it will be possible to obtain a mathematical expression and to compare it continuously to the sound recorded by the machine during the machining process, in order to detect possible deviations.

With the aim of seeing the influence on those IMF components different to the first, the second IMF was studied for experiments 700-15 and 700-45. Figure 9a shows the signal of experiment 700-15 in red, with the second IMF in blue. Figure 9b depicts the HHT of experiment 700-15

with its time-frequency trend as a red line. Figure 9c shows the signal of 700-45 in red dots, its IMF 2 as a blue line, while Figure 9d shows its instantaneous frequency obtained from HHT in blue dots, and its time-frequency trend as a red line.

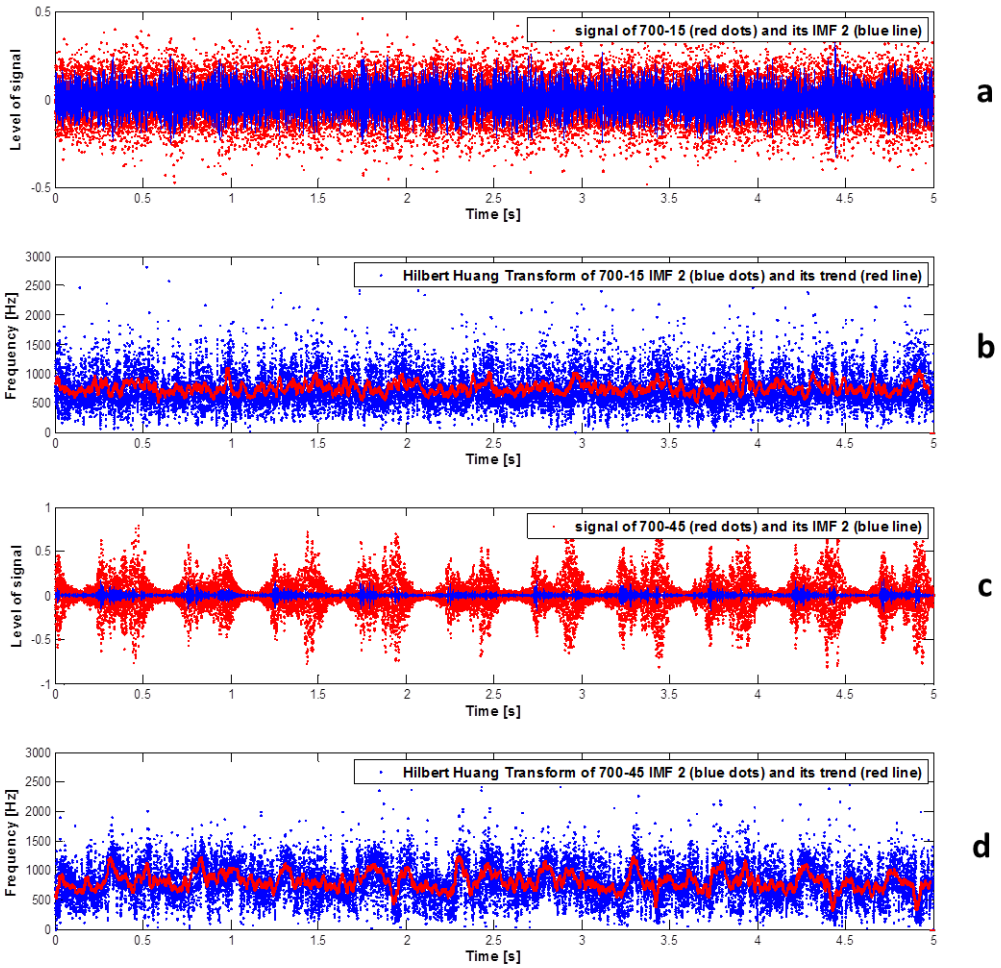

Figure 9. Signal and its IMF2: a) 700-15, c) 700-45; Time-frequency representation over a period of 5 s, corresponding to 2nd IMF component from EMD treatment: b) 700-15, d)700-45

From Figures 9a and 9c it can be appreciated that the second IMF of the 700-45 experiment has a lower amplitude than the second IMF of the 700-15 experiment, in accordance with FFT in Figure 7.

The results are summarized in Table 4, which presents, for every experiment and for the first four IMF components, the IMF power, the % of the IMF power in relation to the total power of

the signal and their average IMF frequency. Table 4 also includes a new parameter S_H that was defined according to Equation 11.

$$S_H = \frac{\sum_{i=2}^{4} EIMFi}{EMF1} \quad \text{(Eq. 11)}$$

Where EIMFi is the energy of the i-th IMF, and EIMF1 is the energy of the first IMF.

Parameter S_H, like parameter S_F, shows the relationship between the energy corresponding to low frequency contained in the IMF 2 to IMF 4 and the energy corresponding to high frequency contained in the IMF 1.

Table 4. Components IMF from Empirical Mode Decomposition (EMD)

Components IMF from Empirical Mode Decomposition (EMD)						S_H
Experiment		IMF 1	IMF 2	IMF 3	IMF 4	$\frac{\sum_{i=2}^{4} EIMFi}{EMF1}$
700-45	Power	0.0255	$6.8e^{-4}$	$3.5e^{-4}$	$2.4e^{-4}$	0.05
	%	99	------	------	------	
	Frequency	1722 Hz	------	------	------	
700-60	Power	0.0287	0.0012	$3e^{-4}$	$2e^{-4}$	0.06
	%	96	4	------	------	
	Frequency	1830 Hz	916 Hz	------	------	
700-30	Power	0.0171	0.0043	0.0024	$6.4e^{-4}$	0.43
	%	75	17	7	------	
	Frequency	1730 Hz	836 Hz	447 Hz	------	
700-15	Power	0.0055	0.0052	0.0023	$5.5e^{-4}$	1.45
	%	40	37	16	------	
	Frequency	1580 Hz	720 Hz	405 Hz	------	

In Table 4 a clear distinction is observed between the 700-15/30 and 700-60/45 experiments, suggesting that, when the energy is mainly concentrated in the first IMF component corresponding to high frequency, as in the 700-60 and 700-45 experiments, then the honing machine processes will function incorrectly because of clogging. This also leads to low S_H values of 0.06 and 0.05 respectively. In contrast, when other IMFs become important, cutting is more appropriate. However, at density 15 the second IMF is almost as important as the first,

suggesting that the number of abrasives is insufficient for cutting properly. This corresponds to an S_H value higher than 1. Thus, the proper cutting operation obtained with density 30 corresponds to S_H values of between 0.1 and 1. This links the acoustic analysis results with the experimental 3D and 2D roughness conclusions.

4. Conclusions

The main conclusions of the paper are summarized as follows:

- According to 2D roughness, material removal rate and tool wear, for grain size 64 and pressure 700 N/cm^2, abrasive density 15 is insufficient, because the material removal rate is low and tool wear is high. Density of 60 is also ruled out since, although roughness and tool wear are low, the material removal rate decreases with respect to density 45, suggesting clogging of the honing stones.

- A more detailed analysis, taking surface topography and areal roughness parameters into account, reveals clogging at density 45, as well as the appearance of non-straight and discontinuous honing marks. For this reason, density 30 is recommended.

- New parameters, S_F and $S_{H,}$ were defined, obtained from the comparison of low and high frequencies in Fast Fourier Transform and Hilbert Huang Transform respectively. The correct cutting operation provided by density 30 is related to S_F and S_H values of between 0.1 and 1.

- The time-frequency analysis by means of Hilbert Huang transform showed that, when density is too low (e.g. 15), the second IMF is almost as important as the first. On the other hand, for high densities 45 and 60 almost all the power is concentrated in the first IMF. For density 30, the first IMF component has a relatively high percentage of power, with less important second and third IMF components.

5. Acknowledgements

The authors thank the Spanish Ministry of Economy and Competitiveness for project number DPI2011-26300. They also thank the company Honingtec for lending the test honing machine.

References

[1] Z.N. Farhat, Wear mechanism of CBN cutting tool during high-speed machining of mold steel, Mater. Sci. Eng. A. 361 (2003) 100–110. doi:10.1016/S0921-5093(03)00503-3.

[2] I.D. Marinescu, M. Hitchiner, E. Uhlmann, I. Inasaki, Handbook of machining with grinding wheels, CRC Press, Boca Raton FL, 2007.

[3] F. Klocke, Manufacturing Processes 2 - Grinding, Honing, Lapping, Springer, 2009. http://www.apress.com/9783540922582 (accessed November 24, 2015).

[4] I. Buj-Corral, J. Vivancos-Calvet, M. Coba-Salcedo, Modelling of surface finish and material removal rate in rough honing, Precis. Eng. 38 (2014) 100–108. doi:10.1016/j.precisioneng.2013.07.009.

[5] V. Balsamo, A. Caggiano, K. Jemielniak, J. Kossakowska, M. Nejman, R. Teti, Multi Sensor Signal Processing for Catastrophic Tool Failure Detection in Turning, Procedia CIRP. 41 (2016) 939–944. doi:10.1016/j.procir.2016.01.010.

[6] X. Li, A brief review: acoustic emission method for tool wear monitoring during turning, Int. J. Mach. Tools Manuf. 42 (2002) 157–165. doi:10.1016/S0890-6955(01)00108-0.

[7] K. Zhu, Y.S. Wong, G.S. Hong, Wavelet analysis of sensor signals for tool condition monitoring: A review and some new results, Int. J. Mach. Tools Manuf. 49 (2009) 537–553. doi:10.1016/j.ijmachtools.2009.02.003.

[8] Q. Liu, X. Chen, N. Gindy, Investigation of acoustic emission signals under a simulative environment of grinding burn, Int. J. Mach. Tools Manuf. 46 (2006) 284–292. doi:10.1016/j.ijmachtools.2005.05.017.

[9] R. Babel, P. Koshy, M. Weiss, Acoustic emission spikes at workpiece edges in grinding: Origin and applications, Int. J. Mach. Tools Manuf. 64 (2013) 96–101. doi:10.1016/j.ijmachtools.2012.08.004.

[10] G. Onwuka, K. Abou-El-Hossein, Surface Roughness in Ultra-high Precision Grinding of BK7, Procedia CIRP. 45 (2016) 143–146. doi:10.1016/j.procir.2016.03.023.

[11] C. Schmitt, S. Klein, D. Bähre, An Introduction to the Vibration Analysis for the Precision Honing of Bores, Procedia Manuf. 1 (2015) 637–643. doi:10.1016/j.promfg.2015.09.056.

[12] M. Kanthababu, M.S. Shunmugam, M. Singaperumal, Identification of significant parameters and appropriate levels in honing of cylinder liners, Int. J. Mach. Mach. Mater. 5(1) (2009) 80–96.

[13] P.J. Loughlin, J.W. Pitton, L.E. Atlas, Construction of positive time-frequency distributions, IEEE Trans. Signal Process. 42 (1994) 2697–2705. doi:10.1109/78.324735.

[14] N.E. Huang, Z. Shen, S.R. Long, M.C. Wu, H.H. Shih, Q. Zheng, et al., The empirical mode decomposition and the Hilbert spectrum for nonlinear and non-stationary time series analysis, Proc. R. Soc. A Math. Phys. Eng. Sci. 454 (1998) 903–995. doi:10.1098/rspa.1998.0193.

[15] J. Chen, Z. Li, J. Pan, G. Chen, Y. Zi, J. Yuan, et al., Wavelet transform based on inner product in fault diagnosis of rotating machinery: A review, Mech. Syst. Signal Process.

70 (2016) 1–35. doi:10.1016/j.ymssp.2015.08.023.

[16] T.A.C.M.Claasen;W.F.G.Mecklenbräuker;, The Wigner distribution—A tool for time-frequency signal analysis—Part I: Continuous time signals, Phillips J. Res. 35 (1980) 217–250. https://www.researchgate.net/publication/257291757_The_Wigner_distribution-A_tool_for_time-frequency_signal_analysis-Part_I_Continuous_time_signals (accessed December 1, 2016).

[17] I. Marinescu, D. Axinte, A time–frequency acoustic emission-based monitoring technique to identify workpiece surface malfunctions in milling with multiple teeth cutting simultaneously, Int. J. Mach. Tools Manuf. 49 (2009) 53–65. doi:10.1016/j.ijmachtools.2008.08.002.

[18] G. Siracusano, F. Lamonaca, R. Tomasello, F. Garescì, A. La Corte, D.L. Carnì, et al., A framework for the damage evaluation of acoustic emission signals through Hilbert–Huang transform, Mech. Syst. Signal Process. 75 (2016) 109–122. doi:10.1016/j.ymssp.2015.12.004.

[19] N. Roveri, A. Carcaterra, Damage detection in structures under traveling loads by Hilbert–Huang transform, Mech. Syst. Signal Process. 28 (2012) 128–144. doi:10.1016/j.ymssp.2011.06.018.

[20] E. Simon Carbajo, R. Simon Carbajo, C. Mc Goldrick, B. Basu, ASDAH: An automated structural change detection algorithm based on the Hilbert–Huang transform, Mech. Syst. Signal Process. 47 (2014) 78–93. doi:10.1016/j.ymssp.2013.06.010.

[21] B. Van Hecke, J. Yoon, D. He, Low speed bearing fault diagnosis using acoustic emission sensors, Appl. Acoust. 105 (2016) 35–44. doi:10.1016/j.apacoust.2015.10.028.

[22] A.A. Mohammed, S.M. Haris, M.Z. Nuawi, Utilizing Hilbert–Huang transform in detection some of mechanical properties of the refractory metals, Mech. Syst. Signal Process. 68–69 (2016) 449–461. doi:10.1016/j.ymssp.2015.07.024.

[23] A.M. Bassiuny, X. Li, Flute breakage detection during end milling using Hilbert–Huang transform and smoothed nonlinear energy operator, Int. J. Mach. Tools Manuf. 47 (2007) 1011–1020. doi:10.1016/j.ijmachtools.2006.06.016.

[24] T. Kalvoda, Y.-R. Hwang, A cutter tool monitoring in machining process using Hilbert–Huang transform, Int. J. Mach. Tools Manuf. 50 (2010) 495–501. doi:10.1016/j.ijmachtools.2010.01.006.

[25] H. Cao, Y. Lei, Z. He, Chatter identification in end milling process using wavelet packets and Hilbert–Huang transform, Int. J. Mach. Tools Manuf. 69 (2013) 11–19. doi:10.1016/j.ijmachtools.2013.02.007.

[26] Y. Fu, Y. Zhang, H. Zhou, D. Li, H. Liu, H. Qiao, et al., Timely online chatter detection in end milling process, Mech. Syst. Signal Process. 75 (2016) 668–688. doi:10.1016/j.ymssp.2016.01.003.

[27] Z. Yang, Z. Yu, C. Xie, Y. Huang, Application of Hilbert–Huang Transform to acoustic emission signal for burn feature extraction in surface grinding process, Measurement. 47 (2014) 14–21. doi:10.1016/j.measurement.2013.08.036.

[28] FEPA, 61/97 - FEPA standard for superabrasives grain sizes, (1997).

[29] ISO, ISO 6104:2005 - Superabrasive products -- Rotating grinding tools with diamond or cubic boron nitride -- General survey, designation and multilingual nomenclature, (2005). http://www.iso.org/iso/catalogue_detail.htm?csnumber=36553 (accessed July 28, 2014).